J. Membrane Biol. 175, 149–160 (2000)

The Journal of
Membrane
Biology

Three Types of Membrane Excitations in the Marine Diatom *Coscinodiscus wailesii*

D. Gradmann,* C.M. Boyd
Department of Oceanography, Dalhousie University, Halifax, N.S., B3H 4J1 Canada

Received: 2 December 1999/Revised: 3 March 2000

Abstract. Three types of electrical excitation have been investigated in the marine diatom *Coscinodiscus wailesii.* I: Depolarization-triggered, transient Cl^- conductance, $G_{Cl}(t)$, followed by a transient, voltage-gated K^+ conductance, G_K, with an active state *a* and two inactive states i_1 and i_2 in series (a-i_1-i_2). II: Similar $G_{Cl}(t)$ as in Type-I but triggered by hyperpolarization; a subsequent increase of G_K in this type is indicated but not analyzed in detail. III: Hyperpolarization-induced transient of a voltage-gated activity of an electrogenic pump (i_2-a-i_2), followed by $G_{Cl}(t)$ as in Type-II excitations. Type-III with pump gating is novel as such. $G_{Cl}(t)$ in all types seems to reflect the mechanism of $InsP_3^-$ and Ca^{2+}-mediated $G_{Cl}(t)$ in the action potential in *Chara* (Biskup et al., 1999). The nonlinear current-voltage-time relationships of Type-I and Type-III excitations have been recorded under voltage-clamp using single saw-tooth command voltages (voltage range: −200 to +50 mV, typical slope: ±1 Vs^{-1}). Fits of the corresponding models to the experimental data provided numerical values of the model parameters. The statistical significance of these solutions is investigated. We suggest that the original function of electrical excitability of biological membranes is related to osmoregulation which has persisted through evolution in plants, whereas the familiar and osmotically neutral action potentials in animals have evolved later towards the novel function of rapid transmission of information over long distances.

Key words: Action potential — Gating model — Parameter identification — Reaction kinetics — Saw-tooth clamp — Voltage clamp

Permanent address: Abteilung Biophysik der Pflanze, Albrecht-von-Haller-Institut für Pflanzenwissenschaften, Universität Göttingen, Untere Karspüle 2, D-37073 Göttingen, Germany

**Correspondence to:* D. Gradmann

Introduction

The behavior of marine diatoms is of global importance as they accomplish >20% of the global CO_2 assimilation (Werner, 1977). However, very little is known about the physiology of these cells, especially the physiology of ion transport. Previous electrophysiological studies on the marine diatoms *Coscinodiscus radiatus* (Gradmann & Boyd, 1995) and *C. wailesii* (Boyd & Gradmann, 1999) have shown that these cells can change between different physiological states within minutes or even seconds. These states comprise excitatory phenomena such as transient hyperpolarizations and depolarizations. Attempts to study these phenomena with patch-clamp techniques have failed so far because of bad seal formation. In addition, plant cells under patch-clamp conditions are frequently under physiological disorder.

However, detailed electrical characteristics, i.e., nonlinear current-voltage-time (*I-V-t*) relationships, of intact cells in specific physiological states can be recorded in the range of a second by application of single saw-tooth voltage-clamp protocols (Gradmann & Boyd, 1999). Records of this type and from traditional step-protocols have been used here to analyze the mechanisms of three types of excitation in *C. wailesii.* In particular, the records from single saw-tooth experiments have been analyzed. Such records allow some direct evaluation. Simple rules for such evaluations have been presented previously (Gradmann & Boyd 1999). Some of these rules will briefly be introduced here again for convenient application. Most important, however, these records from single saw-tooth experiments have been used for a detailed reaction kinetic analysis of the level of fitting the rate constants of Markovian gating models to the experimental data.

The results provide new insights in the general issue of excitability in biological membranes.

Materials and Methods

Cells and electrophysiological setup have been described previously in detail (Boyd & Gradmann, 1999). Briefly, cylindrical cells of the marine diatom *C. wailesii* have been used because of their large size (radius about 100 μm, altitude about 100 μm in rare cases up to 200 μm). Voltage-clamp experiments have been carried out using a voltage clamp-circuit (Dagan 200 TEV) and double-barreled microelectrodes for voltage recording and for current injection.

Data acquisition and control of the voltage-clamp circuit was carried out via an AD/DA converter (Keithley System 500 KDAC). Personal computers have been used to run custom-tailored software for AD/DA conversion and for data processing. The time courses of the transmembrane voltage, V (free running or under voltage-clamp control) and of the clamp current, I, were recorded on the computer. Simultaneously, the results have continuously been displayed with high temporal resolution on a digital oscilloscope, and recorded with low temporal resolution on a strip chart recorder for immediate inspection and for convenient scanning of the results.

Typical voltage-clamp experiments followed single saw-tooth command voltages, starting with a reference voltage V_0 (usually close to the free running V), followed by a ramp from V_0 to a minimum voltage V_1 (usually −200 mV), a second ramp (ascending branch) from V_1 to a maximum voltage V_2 (usually +50 mV), and a third ramp from V_2 back to V_0. The first and third ramps form the descending branch. Immediately before and after the ramps, V was clamped at steady state V_0 for 20 msec.

With respect to the recorded currents of some 100 nA, the usual ramp slope S_r of 1 Vs^{-1} was slow enough to ignore the capacitive current $I_C = C \cdot S_r \approx 2$ nA in normal cells of *C. wailesii* with a surface area of about 0.2 mm^2, and a standard specific membrane capacitance of about 10 mF m^{-2}.

Theory

Electroenzymes are proteins which catalyze the movement of the net electrical charges through lipid membranes; their activity is frequently sensitive to the transmembrane voltage, V. The simplest equivalent circuit for a crude description of the electrical properties of the plasmalemma of plant cells consists of three major electroenzymes operating in parallel (Boyd & Gradmann, 1999): a predominant pathway for K^+ diffusion with the equilibrium voltage E_K, an electrogenic pump ($E_P \ll E_K$) which is required to explain $V < E_K$, and diffusion pathways for Cl^- ($E_{Cl} \gg E_K$) which can account for $V > E_K$. For the description of the V-sensitive activity of an electroenzyme, the simplest model, *a-i*, consists of an active state *a* and an inactive state *i* with the transition probabilities k_{ia} and k_{ai} which depend on V in the form $k_{ia} = k_{ia}^0 \exp(d_{ia}u)$ and $k_{ai} = k_{ai}^0 \exp(d_{ai}u)$, where the superscript ^{0} marks the transition probability at zero V, d_{ia} and d_{ai} are V-sensitivity coefficients, and $u = VF/(RT)$ is the normalized membrane voltage. In a different context, the V-sensitivity of all electroenzymes in the plasmalemma of plant cells has been crudely approached by such two-state gating schemes, *a-i*, except for the Cl^- conductance for which a three-state gating scheme, i_1-*a*-i_2, has been employed (e.g., Mummert & Gradmann, 1991, Gradmann, Blatt & Thiel, 1993, Gradmann & Hoffstadt, 1999). In the present work, the two-state gating schemes turned out to be insufficient to describe the kinetics of the K^+ conductance and of the pump activity. Therefore a general three-state gating scheme, *1-2-3*, has been used, with $1 = a$, $2 = i_1$ and $3 = i_2$ for the K^+ conductance and $1 = i_1$, $2 = a$ and $3 = i_2$ for the pump. Initially, the gating scheme for the Cl^- conductance was also $1 = i_1$, $2 = a$ and $3 = i_2$ as in the previous studies. For the present study, however, a V-insensitive Cl^- conductance, G_{Cl}, turned out to be sufficient.

On the other hand, G_{Cl} was not constant but seemed to depend on a factor X ($G_{Cl} = XG_{Cl,max}$; $0 < X < 1$), which appeared and disappeared. For the description of the electrical excitation in *Chara*, this gating factor X for the G_{Cl} has recently been identified (Biskup, Gradmann & Thiel, 1999). In these cells the gating factor is a certain amount of Ca^{2+} which can suddenly be released by a V-sensitive, phospholipase-C-mediated mechanism from $InsP_3$-sensitive internal stores into the cytoplasm, where it causes a transient increase of the concentration of free Ca^{2+} before it disappears again into a global buffering system (Biskup et al., 1999). By analogy to these relationships in *Chara*, the kinetics of the transient G_{Cl} is described here by a V threshold V_X. When V crosses this threshold, X is released with the rate constant k_r and buffered away again with the rate constant k_b; this yields a time course

$$X(t) = \frac{k_r}{k_r - k_b}\left(\exp(-k_b t) - \exp(-k_r t)\right) \tag{1}$$

which, in turn, determines $G_{Cl}(t) = G_{Cl,max}\, X(t)$.

The currents through the three electroenzymes are: The pump current,

$$I_P = p_{Pa} G_{P,max}\,(V - E_P), \tag{2}$$

with the actual pump activity p_{Pa} ($0 < p_{Pa} < 1$) and a maximum (linear) pump conductance, $G_{P,max}$; the K^+ current,

$$I_K = p_{Ka}\, g_K^0\, (c_{Ki} - c_{Ko} \exp(-u))/(1 - \exp(-u)), \tag{3}$$

with the actual activity p_{Ka} ($0 < p_{Ka} < 1$) of the K^+ conductance, a maximum K^+ conductance $g_K{}^0$ under reference conditions, i.e., at 1 M internal and external K^+ concentrations, c_{Ki} and c_{Ko} respectively; and finally the Cl^- current in the simple form

$$I_{Cl} = G_{Cl} V \tag{4}$$

which implies E_{Cl} to be near 0 mV (Boyd & Gradmann, 1999).

For the calculations of the changing activities p_{Ka} and p_{Pa}, the common three-state gating model, *1-2-3*, has been used, with the four rate constants (transition probabilities) k_{12}, k_{21}, k_{23} and k_{32} which depend on the actual V in the form

$$k_{ij} = k_{ij}{}^0 \exp(d_{ij}u) \tag{5}$$

again; $k_{ij}{}^0 = k_{ij}$ at $V = 0$, and the corresponding V-sensitivity factors d_{ij}. At a given V, the steady-state occupancies of the three states are

$$p_1 = k_{32}k_{21}/den, \tag{6a}$$

$$p_2 = k_{12}k_{32}/den, \tag{6b}$$

$$p_3 = k_{12}k_{23}/den \tag{6c}$$

with the denominator $den = k_{32}k_{21} + k_{12}k_{32} + k_{12}k_{23}$. Upon a change in V, k_{ij} assume new values according to Eq. 5; and the three occupancies change within a small time interval Δt by the amounts

$$\Delta p_1 = (-k_{12}p_1 + k_{21}p_2)\Delta t, \tag{7a}$$

$$\Delta p_2 = (k_{12}p_1 - (k_{21} + k_{23})p_2 + k_{32}p_3)\Delta t, \tag{7b}$$

$$\Delta p_3 = (k_{23}p_2 - k_{32}p_2)\Delta t. \tag{7c}$$

These relationships allow an iterative calculation of the time course of the total current ($I_t = I_P + I_K + I_{Cl}$) in response to any time course of command V under V clamp.

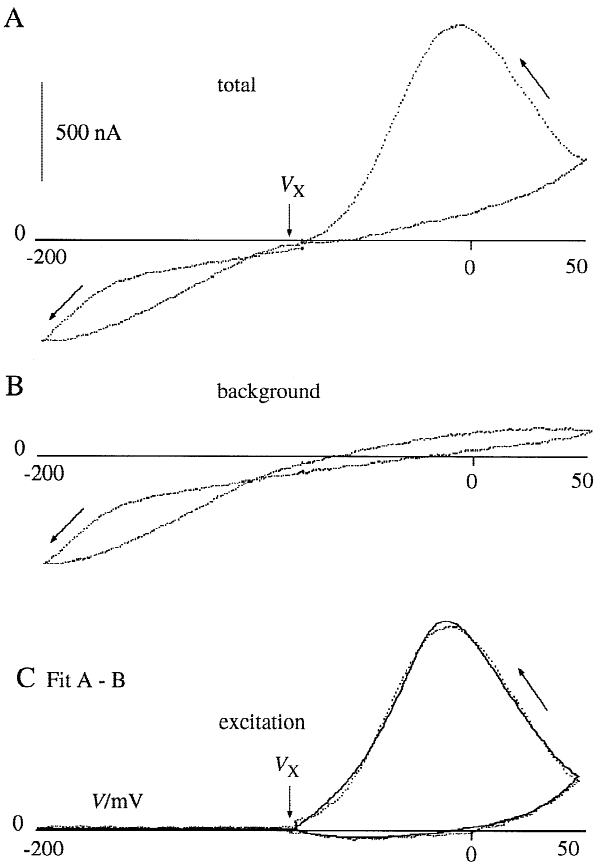

Fig. 1. *I-V-t* relationship of Type-I excitation in *C. wailesii;* single saw-tooth *V*-clamp recordings, start *V:* −80 mV; ramp speed: ±1 Vs^{-1}; arrows indicate temporal direction of recording; (*A*) Recording in excitable state 60 sec after last excitation; (*B*) Background recording in recovery state 6 sec after last excitation (*A*); (*C*) Current differences between recording *A* and *B*, displaying isolated *I-V-t* relationship of Type-I excitation; dots recorded, line fitted with *V*-triggered G_{Cl} transient (V_X*:* trigger point) and *V*-gated G_K with three-state (*1-2-3*) gating model ($1 = a$, $2 = i_1$, $3 = i_2$); parameters listed in Table 1, start configuration for fit: 1111 in Table 1.

A computer program has been developed for these model calculations under single saw-tooth clamp protocols, including automatic fitting of selected model parameters for best agreement between simulated and measured data. During the fitting routine, the selected parameters are changed by a small increment, starting with ±1 or ±0.1%; $\sigma = (\sum(\overline{X} - X_i)^2)^{0.5}$ has been used as a measure of the fit quality; cycles of adjusting all parameters are repeated until σ does not fall anymore; then, the increment is divided by 2, and the procedure is repeated until the increment falls below the stop criterion, e.g., 0.1 or 0.01%. Compared to familiar gradient algorithms (e.g., Simplex), this routine is slower but finds better solutions in ambiguous multiparameter fits. The software is written in Turbo-Pascal and is available on request.

Results and Discussion

Three types of electrical excitation (Type-I, -II, and -III) are reported here. In 52 cells, 8 exhibited Type-I excitations, 3 cells showed Type-II, and Type-III has been observed in 5 cells. Here, typical examples are presented.

Type-I: Depolarization-triggered Increase of G_{Cl}, followed by Increase of G_K

The characteristics of this type are illustrated in Fig. 1. Panel *A* shows the total current response of an excitable cell under single saw-tooth *V*-clamp conditions > 60 sec after the last excitation. Panel *B* shows the response of the same cell upon the same clamp conditions, but 6 sec after the last excitation (*A*). Under these conditions the cell is in a nonexcitable, recovery state, and provides the background currents for isolation of the excitation currents (*C*) from the total current (*A*). The background (*B*) comprises all electrical processes that do not participate in the excitation mechanism. The dots in Fig. 1*C* display the experimental data of the current differences between the recordings *A* and *B.* The line in Fig. 1*C* is the result of fitting a model to the experimental data. As explained in the Theory section, the excitation model consists of a Cl^- conductance, $G_{Cl} = G_{Cl,max}X$, with a constant $G_{Cl,max}$ (10 nS) and a transient appearance of *X* which starts in excitable cells at a depolarization beyond a threshold voltage, V_X. The assumed $G_{Cl,max}$ of 10 nS actually reflects the product of a true $G_{Cl,max}$ and an $X_{max} \leq 1$. The time course $X(t)$ is determined by the two rate constants k_r for release and k_b for buffering (*see* Eq. 1).

The qualitative reason for using this model for the behavior of G_{Cl} instead of a three-state gating scheme of the familiar i_1-*a*-i_2 type, is the discontinuous onset of the G_{Cl} during the depolarization. This 'kink' has already been pointed out previously (Gradmann & Boyd, 1999). It is, however, not excluded here that G_{Cl} in *C. wailesii* is *V*-gated as in the plasmalemma of other plant cells. It is only for the sake of simplicity of the model that this feature has not been considered here. The coincidence between fit and measured data does not call for further refinement of the G_{Cl} model.

It should be noted that, in the present recordings, it was only coincidental that the threshold V_X for the sudden onset of G_{Cl} during the continuous change of the *V* from −200 to +50 mV, is almost exactly at the resting *V* (≈ −80 mV), which has been taken as the reference *V* (holding *V*, V_0) before and after the *V* ramps. The average V_X from 7 cells was −78 ± 17 mV (SD).

The behavior of G_K is well described with the serial (*1-2-3*) three-state gating model *a*-i_1-i_2. Simple outward rectifying gating of the *a-i* type does not satisfy the measured data, especially because of a peculiarity on the right hand side of Fig. 1*C*, at the beginning of the descending *V* branch. Here the current still rises in an accelerated mode, causing an inflection point in the total rise towards the peak current. This observation can be

Table 1. Stability of fitted k values with respect to configuration of start values in fits of gating scheme *1-2-3* for G_K: *1 = a, 2 = i_1, 3 = i_2;* for data in Fig. 1*C*

Parameter Ref.	Gated G_K				G_{Cl} transient			
	k^0_{12}	k^0_{21}	k^0_{23}	k^0_{32}	k_r	k_b	σ_{start}	σ_{stop}
	1	10	50	0.05	10	10		
Start confg.								
Fitted								
1111	1.4	7.7	52	0.033	9.3	8.1	288	10.1
2111	2.6	7.4	54	0.036	9.6	9.3	263	10.1
1211	1.7	11.3	50	0.023	7.1	9.0	767	11.0
2211	2.8	11.5	50	0.024	8.9	10.5	725	10.1
1121	1.4	8.4	53	0.030	10.2	10.0	151	10.2
2121	2.2	8.1	55	0.033	10.4	10.1	130	10.2
1221	1.4	12.2	49	0.021	10.2	10.0	532	10.3
2221	1.4	11.6	51	0.023	10.4	10.1	493	10.2
1112	1.7	5.5	55	0.048	7.4	9.0	812	10.9
2112	3.0	5.5	56	0.051	8.5	9.2	764	10.4
1212	1.6	9.1	52	0.028	7.5	9.0	1719	10.8
2212	2.5	9.4	52	0.029	7.9	9.1	1637	10.6
1122	1.3	6.7	54	0.038	10.0	10.0	545	10.3
2122	2.3	6.0	56	0.045	10.4	10.2	502	10.3
1222	1.1	10.2	50	0.024	7.3	9.0	1274	10.9
2222	2.1	7.6	53	0.035	8.0	9.0	1198	10.5
111121	1.4	7.5	52	0.034	11.6	9.0	289	10.0
111112	1.4	8.7	53	0.029	10.2	10.1	290	10.3
means (1111 to 2222)	1.9	8.6	53	0.033	8.9	8.5	736	10.4
SD/%	31	25	4	3	14	7	67	3

k in s^{-1}; σ in nA; code for configuration of start parameters: factors of standard configuration, e.g., 2112 means $k^0_{12} = 2$, $k^0_{21} = 10$, $k^0_{23} = 50$, and $k^0_{12} = 0.1$ sec^{-1}; in 111121 and 11112, start parameters of k_r and k_b have also been doubled, respectively; fixed parameters: $g^0_K = 10$ mS M^{-1} (c_{Ki}: 0.4 M, c_{Ko}: 0.01 M), $d_{12} = 1$, $d_{21} = -1$, $d_{23} = -1.5$, $d_{32} = 2.5$, $G_{Cl,max} = 10$ nS, $V_X = -80$ mV; start increment: ±1%, stop increment: ±0.1%.

described by assuming two steps of *V*-gating with different sign and amount of the gating charges d_{12}-d_{21} and d_{23}-d_{32}. Different temporal behavior of the two steps is of course intrinsic due to Eqs. 5 and 7 and a matter of the k^0 values. Preliminary fits (trial and error with numerous combinations of start parameters, start increment 0.1%, stop increment <0.01%) of the G_K behavior by a constant $G_{K,max}$ and ten free parameters (four k^0s, four ds, k_r and k_b) resulted in good ($9 < \sigma < 10$) but ambiguous solutions which converged to the following d values: $d_{12} \approx 0.8$, $d_{21} \approx -1.0$, $d_{23} \approx -1.5$, and $d_{21} \approx 2.5$. To reduce ambiguities, rounded d values ($d_{12} = 1$, $d_{21} = -1$, $d_{23} = -1.5$, and $d_{21} = 2.5$, yielding gating charges of $d_{12} - d_{21} = 2$, and $d_{23} - d_{32} = -4$) have been used as fixed parameters in systematic fits to determine the four k^0s, k_r and k_b.

In principle, from ideal, noise-free data as in Fig. 1*C*, the fit algorithm is able to determine the four k^0s, k_r and k_b when the other parameters (V_X, $G_{P,max}$, c_{Ki}, and the d values) are fixed. However, the real data are noisy and introduce ambiguities to the solutions. To assign specific confidence intervals to each of the determined parameters, systematic fits (start increment 1%, stop increment 0.1%) with various start parameters have been carried out to describe the data in Fig. 1*C*.

Beginning with an empirical set of start parameters 1111 in Table 1, the sixteen combinations of initial and/or doubled start parameters have been tested for the effect on the fit quality. The results in Table 1 show that the quality (measured by σ) of the start configuration does not necessarily correlate with the quality at the end of the fit procedure. For instance, configuration 1121 starts with a relatively small σ_{start} (151 pA) compared with configuration 1212 ($\sigma_{start} = 1718$ pA) but ends with a greater σ_{stop} (10.26 pA) compared with $\sigma_{stop} = 10.18$ pA of 2121. Under these circumstances the parameter values of the best fit are not necessarily the closest ones to the true values, despite the fact that the real reaction system can be expected to be more complex than the apparent minimum reaction scheme investigated. Nevertheless, the data in Table 1 provide a realistic scope of the relationships.

Fifteen out of the sixteen start configurations pre-

Table 2. Differential sensitivity of S of fit quality on changes of individual parameters of model for Type-I excitations

Gated G_K										G_{Cl} transient		
Par.	g_K^0	k_{12}^0	d_{12}	k_{21}^0	d_{21}	k_{23}^0	d_{23}	k_{32}^0	d_{32}	G_{Cl}	k_r	k_d
S	40	1.5	35	1.1	25	6.5	38	6	490	3	0.8	2.5

Reference parameters fitted with start configuration 1111 (s. Table 2); S: arithmetic mean of increase in σ (‰) upon a ±1% change of particular parameter value.

sented lead to fits of very similar, high quality ($10.15 < \sigma < 10.30$) but dissimilar numerical solutions, showing maximum scatter (≈36%) in $k_{12}{}^0$ and minimum scatter in $k_{23}{}^0$ (≈1%).

The stability of the solution can also be characterized by the sensitivity of the quality (here measured by σ) with respect to changes of individual parameters. The results from free and fixed parameters are listed in Table 2. The larger sensitivity of σ to G_K (4.1) compared to G_{Cl} (0.3) simply corresponds to the ratio of these conductances which is qualitatively reflected by the large outward currents mainly carried by K^+ and the small inward currents exclusively carried by Cl^-. The high sensitivity of σ to all *d* values corresponds to their exponential effect on the *k* values (Eq. 5).

As for the *k* values themselves (represented by the k^0 values), the transitions between the two inactive states i_1 and i_2 reflected by k_{23} and k_{32} have more impact on the shape of the *I-V-t* relationships than k_{12} and k_{21} which reflect the direct transitions between active, *a*, and inactive, i_1.

A trial using the mean solution in Table 1 as the start configuration for a further improvement (with a start increment of 0.1% and a stop increment 0.01%, all parameters free), failed: σ_{start} was significantly increased (26 nA), and σ_{stop} did not fall below 9.5 nA.

Figure 2 shows the fits of differences curves (*dI-V-t*) of six experiments from the same cell investigated in Fig. 1. The fits of the excitation loops in the right hand parts of the tracings may have suffered a little bit by slight systematic tilts (change of a linear conductance) in these original data, e.g., clockwise in tracing *A*, virtually absent in *E* (= Fig. 1*C*), and counterclockwise in *F*. Nevertheless, the fits coincide well with the data. The sets of fitted parameters (same start configuration) for all six recordings are listed in Table 3.

It is pointed out that the smallest amplitude of Fig. 2*C* was obtained only 27 sec (recovery time, t_r) after the last excitation (Fig. 2*B*); also the maximum amplitude (Fig. 2*D*) correlates with the maximum t_r of 70 sec in this series of recordings; after a standard recovery time of 60 sec, the current responses have been very similar. Due to intrinsic characteristics of the model, the values of the fitted parameters for each tracing (Table 3) do not correlate in a one-to-one mode with individual observable parameters such as the maximum, or its location, which are determined by several, or even all parameters; correspondingly the degree of recovery is not reflected by an individual parameter. One might have expected that the recovery time is the time of regeneration of *X* (internal, $InsP_3$-sensitive Ca^{2+} stores according to Biskup et al., 1999) which might be reflected by changes of the apparent value of k_r, because this apparent k_r may be the product $Xk_r{}^0$ with a variable *X* and a fundamental $k_r{}^0$ = const. However, such a correlation between t_r and k_r cannot be identified in these data of Fig. 2 and Table 3.

In Fig. 2 the amplitudes of the (outward) K^+ currents exceed the amplitudes of the (inward) Cl^- currents. This asymmetry is due to the experimental conditions. Under conditions of free running voltage, however, the sum of all currents is zero. This means in our case (where only two ion species are involved and capacitive currents can be ignored) that under free running voltage, $I_{Cl} = -I_K$ at any time.

Type-II: Hyperpolarization-triggered Increase of G_{Cl}

Figure 3 compiles the events during a recording which lasted almost 5,000 sec. During this time the cell was hyperpolarized 35 times from the free-running *V* between −50 and −70 mV to a fixed clamp *V* of −80 mV. Starting from an arbitrary time zero, initial times of *V*-clamp episodes are marked in seconds in Fig. 3. No correlation could be detected between the free-running *V* and the characteristic time course of the current upon the hyperpolarization step. In about 50% of the events, the response was negligible (<20 nA, e.g., at 154, 1030, 3946, and 4051 sec), or minute (about 30 to 50 nA, e.g., at 322, 394, 756, 1698, and 1882 sec). In another 25% (e.g., at times 881, 3610, 4526 and 4843 sec), small transient current peaks of up to 300 nA occurred after about 5 sec and relaxed with a time constant of about 10 sec. The remaining 25% of the events consisted of large transients of inward currents with peaks of 0.5 to 1.5 μA at 10 to 20 sec after the *V* step and a duration (time between the two passages of passing half the amplitude) of 20 to 60 sec. In many of these recordings (e.g., at times 197, 494, 2239, 3053, and 3341), the abrupt onset of the inward current did not occur immediately upon the *V* step but with a delay of about a second of the 'minute'

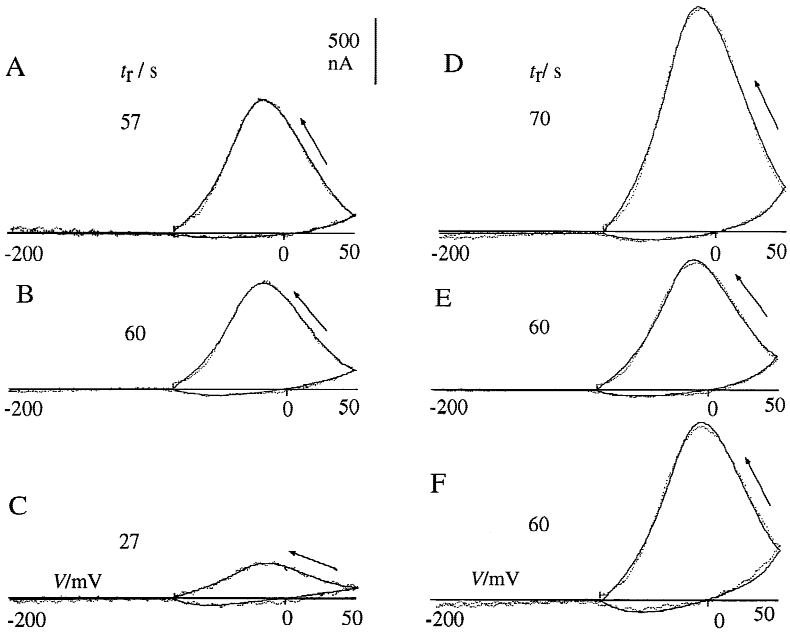

Fig. 2. Series of *I-V-t* relationships of Type-I excitation from one cell of *C. wailesii;* measurement and fits as in Fig. 1*C* (= 2*E*), model parameters for fits in Table 1; t_r: time recovery from last excitation.

Table 3. Model parameters for Type-I excitations from six (*A* to *F*) consecutive events recorded from one cell, values determined from fits of differences as in Fig. 1*C*

Start	Gated G_K				G_{Cl} transient			
	k^0_{12}	k^0_{21}	k^0_{23}	k^0_{32}	k_r	k_b	σ_{start}	σ_{stop}
	1	10	50	0.05	10	10		
Fig. 2								
A	11.6	3.5	29	0.046	3	11	410	10
B	31.2	2.9	26	0.044	6	15	446	7
C	0.8	3.7	19	0.008	7	33	534	6
D	1.6	7.5	45	0.033	6	9	281	14
E	1.4	7.7	52	0.033	9	9	288	10
F	1.1	7.7	56	0.027	13	8	347	17

k in sec^{-1}; σ in nA; gating scheme *1-2-3* for G_K: *1 = a, 2 = i_1, 3 = i_2;* fixed parameters: g^0_K = 10 mS M^{-1} (c_{Ki}: 0.4 M, c_{Ko}: 0.01 M), d_{12} = 1, d_{21} = −1, d_{23} = −1.5, d_{32} = 2.5, V_X = −80 mV, $G_{Cl,max}$ = 10 nS; start increment: ±1%, stop increment: ±0.1%.

type of response. These large current transients comprise another type (Type-II) of electrical excitation. It is obviously triggered by hyperpolarization and consists of a transient Cl^- conductance which is initiated again by a sudden event about 1 sec after the hyperpolarizing *V*-step. Because of the current sign, these currents at −80 mV have to be carried by Cl^- and cannot be due to an increased G_K ($E_K \approx -90$ mV) or a pump activity ($E_P \ll E_K$). In principle, Ca^{2+} and Na^+ are possible candidates as well (E_{Ca} and $E_{Na} \gg -80$ mV) because hyperpolarization-induced G_{Ca} has already been reported from other plant cells (Grabov et al., 1998). However, such dramatic uptake would be a severe load for the homeostasis of low cytoplasmic $[Na^+]$ and even more for $[Ca^{2+}]$ (e.g., the event at 3053 sec reflects >0.1 M cellular valences under *V*-clamp — not at free running *V*, of course). Moreover, the abrupt onset of the transient is characteristic of transient increases of G_{Cl} in *C. wailesii,* as quantitatively demonstrated for the Type-I excitations above and for the Type-III excitations below. The lag of about 1 sec time between the triggering *V*-step and the onset of the G_{Cl} transient, may reflect the $InsP_3^-$ and Ca^{2+}-mediated signal transduction between a *V*-stimulus and G_{Cl} as described for the action potential in *Chara* (Biskup et al., 1999).

When the clamp current at the 4306 sec experiment was recognized as the dramatic type, the clamp-circuit was turned off and the course of the free-running *V* in this excited state of the cell has been recorded. The result is shown in the inset (lower right corner) of Fig. 3. In this tracing, the shoulder during the repolarization may indicate the onset of an increase in G_K, driving *V* towards E_K. In this case, Type-II excitations are very similar to Type-I excitations analyzed above, with the only major difference that the G_{Cl} transient is triggered by depolarization in Type-I and by hyperpolarization in type II. Hyperpolarization-induced excitations have already been reported to occur in *Chara* (Ohkawa & Kishimoto, 1975).

Type-III: Hyperpolarization-induced Increase of Pump Activity and G_{Cl}

Transient hyperpolarizations to $V \ll E_K$ have been reported (Gradmann & Boyd, 1995, Boyd & Gradmann, 1999) to occur in *Coscinodiscus* spontaneously. Two of

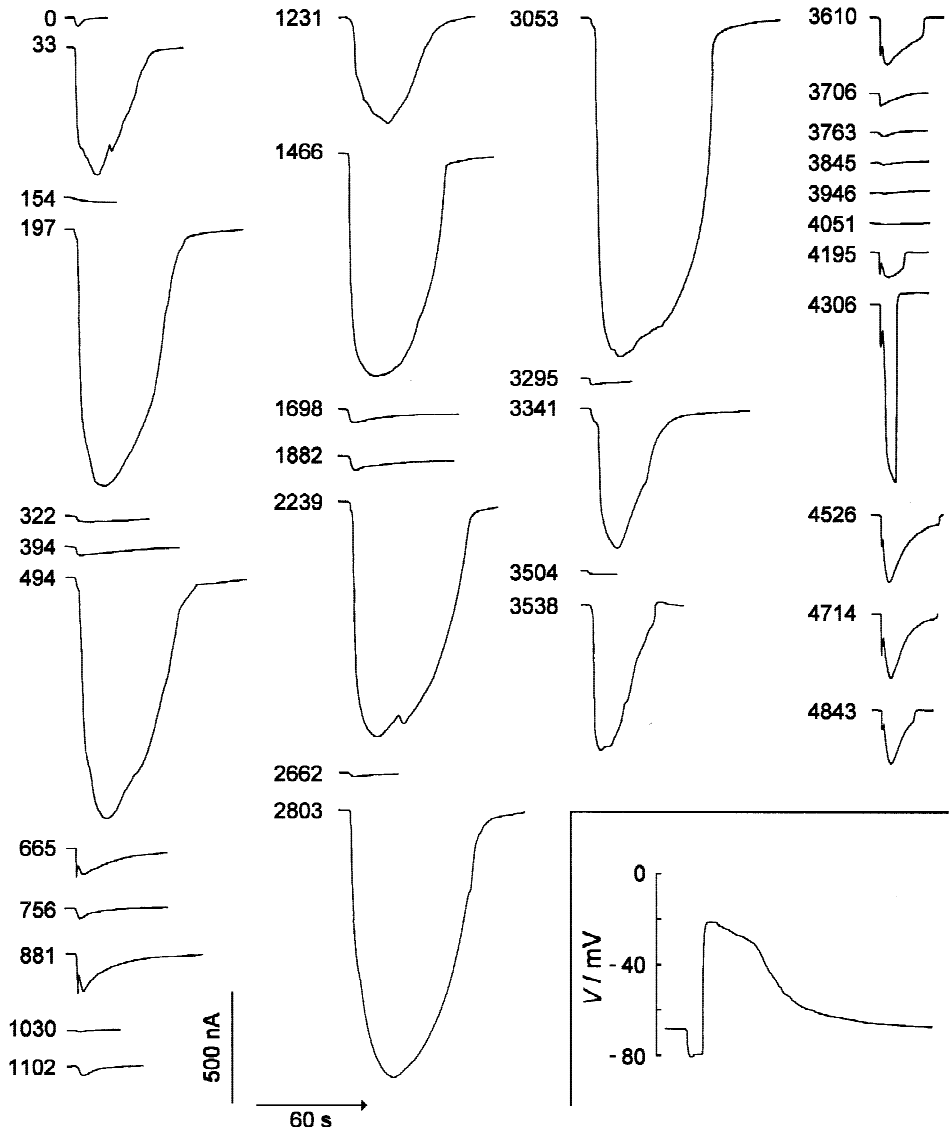

Fig. 3. Series of current responses of *C. wailesii* to *V*-clamp steps from free-running *V* (−50 to −70 mV) to −80 mV; numbers in seconds mark temporal distance from arbitrary zero time; inset lower right corner: excitatory time course of free-running *V* upon clamp-off in experiment 4306 when current maximum under *V*-clamp has been reached.

these events are replotted from (Boyd & Gradmann, 1999) in Fig. 4. From part of these recordings, simultaneous resistance measurements have already suggested that these transient hyperpolarizations are accompanied by a transient increase of a passive ion conductance (Boyd & Gradmann, 1999). *I-V-t* recordings are not available from these events. However, the *I-V-t* recordings shown in Fig. 5*A–C* do allow a detailed analysis of an electrophysiological state which is considered to be equivalent to these transient hyperpolarizations in Fig. 4, only in a subthreshold degree of expression. The two tracings in Fig. 5*A* and *B* have been recorded about one minute apart from the same cell. The difference, *D*, between these tracings shows that within this minute a transient outward current has developed which can be assigned to an electrogenic pump already demonstrated to reside in *C. wailesii* (Gradmann & Boyd, 1995, Boyd & Gradmann, 1999). Figure 5*D′* shows the important features in more detail. Intersections of such *I-V-t* loops identify the equilibrium *V* of the ion transporter which changes its activity — if the background transporters are time-invariant (Gradmann & Boyd, 1999). This intersection appears at about −170 mV in Fig. 5D′. Furthermore, at the negative turning point of the saw-tooth command *V* (here −200 mV), the amount of the arriving current is greater than of the leaving current. This relationship indicates that the activity of the observed ion transporter is decreasing at this point (Gradmann &

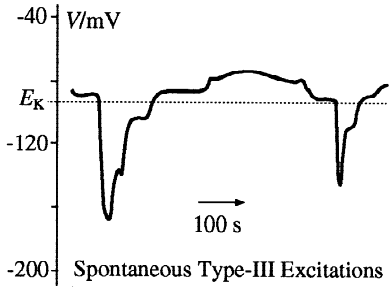

Fig. 4. Time course of free-running *V* of spontaneous Type-III excitation in *C. wailesii:* transient hyperpolarizations to $V \ll E_K$; two consecutive events from one recording replotted from Boyd and Gradmann (1999).

Boyd, 1999). This means that the activity of the pump is first stimulated by the hyperpolarization and then inhibited by an excessive *V* of the same sign. So the decrease of the current I_P after the peak is not only due to a smaller driving force (V-E_P) when *V* approaches E_P but also due to a decrease of the activity (occupancy p_{Pa} of state *a* in gating scheme of pump).

If this transient pump current would cause the small positive humps in Fig. 5*A–C* to cross the *V*-axis (either by more pump activity or by less background conductance, or both), the free-running *V* could be expected to perform spontaneous, transient hyperpolarization such as in Fig. 4.

For a reaction kinetic description of these relationships, the linear three-state gating scheme (*1-2-3*) has been applied to the pump with $1 = i_1$, $2 = a$, $3 = i_2$. A minimum of two inactive states (i_1 and i_2) is required because negative *V* causes first an increase in activity (transition from i_1 to *a*) and later *a* decrease (transition from *a* to i_2). The four fundamental rate constants k_{ij}^0 and the corresponding *V*-sensitivity coefficients d_{ij} (Eq. 5) have initially been estimated by trial and error. In ambiguous cases, smaller amounts of *d* have been preferred. For the sake of simplicity, the *d* values have been changed in steps of 0.5, maintaining integer gating charges d_{12}-d_{21} and d_{23}-d_{32}. With these conditions, reasonable approaches could only be obtained with $d_{12} = -1$, $d_{21} = 1$, $d_{23} = -0.5$, $d_{32} = 0.5$. From these approaches which converged to a similar small σ (and to E_P of about −165 mV consistently, of course) an arbitrary one has been chosen again as a reference set of start parameters (s. Table 4). In analogy to the fits of Type-I excitations above, the four k^0 values could be fitted precisely from noise-free data when the other parameters (E_P, $G_{P,max}$, and the *d* values) are fixed. However, ambiguities of the solutions are introduced by the scatter of the data. A good result is shown in Fig. 5*D* and *D′* (lines coincide well with data); the corresponding model parameters are listed in Table 5. For the fits in Fig. 5*D–G*, only current differences at $V \leq -80$ mV have been used in order to eliminate minor events (probably change in K^+ outward rectifier) at more positive *V* from the present analysis of the events at negative voltages; i.e., the apparent discrepancies between fit and measurement at the positive end of the *V*-axis are not reflected by the numerical statistics.

The changes during the minute between recording Fig. 5*B* and *C* comprise a (negligible) increase of the activity of the pump again, disappearance of a linear leak conductance, $G_L \approx 1$ μS, (illustrated in Fig. 5*E*), and a transient Cl^- conductance, $G_{Cl}(t)$ which is illustrated together with the leak compensation in Fig. 5*F*. G_L has been determined directly and used as a fixed parameter in the consecutive fits. As in Type-I excitations above, $G_{Cl}(t)$ in Type-III excitations have initially been fitted by a linear three-state *V*-gating scheme (*1-2-3*). These trials failed again because of the abrupt onset of the increase in G_{Cl}. So the transient appearance of a factor *X* has been assumed again which is triggered by *V* passing a threshold V_X, this time in the course of hyperpolarization. With a few trials $V_X = -180$ mV could be determined directly again from the data and be used as a fixed parameter for the following fits. The time course of $G_{Cl}(t) = G_{Cl,max}X(t)$ was fitted with a fixed $G_{Cl,max}$ (= 10 nS) and Eq. 1. Again, the apparent $G_{Cl,max}$ reflects the product of a real $G_{Cl,max}$ and an $X_{max} \leq 1$. The current differences between Fig. 5*C* and 5*A* are well described with fixed values of V_X, $G_{Cl,max}$, and G_L, plus the fitted values of k^0, k_r and k_b (*see* Table 4).

It should be mentioned that the transient increase in G_{Cl} proposed here cannot be replaced by a corresponding increase in G_K, because the current tracing of the ascending *V* ramp would have crossed the current tracing of the descending ramp in $E_K \approx -90$ mV.

Finally, panel *G* in Fig. 5 shows the fit of the total difference between the recordings *C* and *A.* This fit does not exactly represent the sum of panels *D* and *F* but a slightly different fit of all six free parameters (k_{12}^0, k_{20}^0, k_{23}^0, k_{32}^0, k_r and k_b) to the total changes between panel *A* and *C*, including a slight increase of the pump activity between *B* and *C* which has been ignored in the first place. The numerical results are listed in Table 5.

The use of the mean parameters as start parameters for further improvement of the fits was successful here, in contrast to the vain attempts discussed above for Type-I analyses. As listed in Table 5 under (*C-A*)′, these means correspond already to an improved σ_{start} (15.0 nA), and σ_{stop} went down to 7.44 nA when all parameters were free. The corresponding line is shown in Fig. 5*G*. This fit needed about 3 hr computing time. Therefore, systematic attempts to investigate the statistical significance of the results have been omitted. After all, the numerical results did not deviate extraordinarily from the coarse but systematic fits in Table 4.

The numbers in Table 4 indicate that some param-

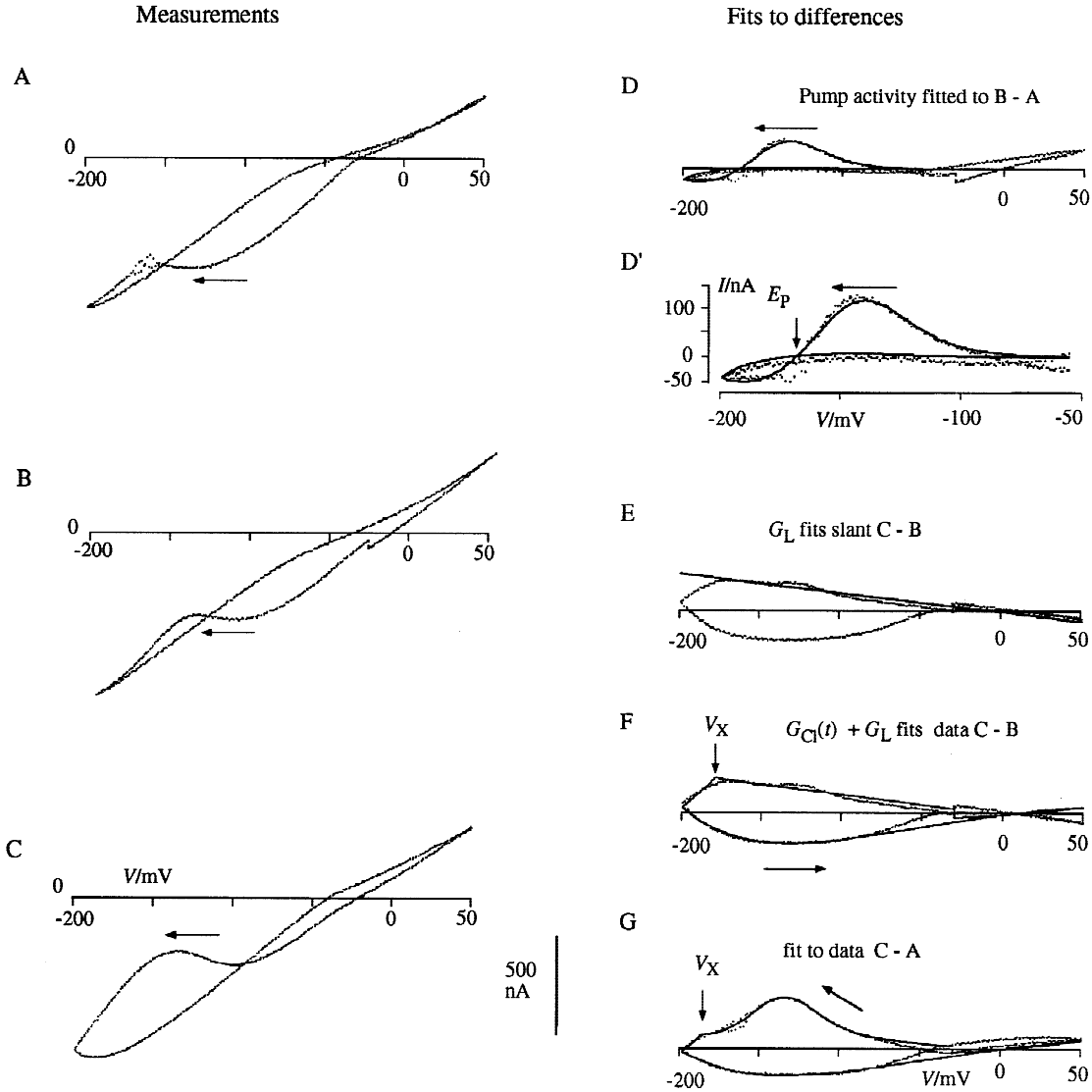

Fig. 5. *I-V-t* relationship of Type-III excitation in *C. wailesii;* single saw-tooth *V*-clamp recordings, start *V:* −80 mV; ramp speed: ± *V* sec^{-1}; arrows indicate temporal direction of recording; (*A*) original recording with conspicuous loop in negative *V* range (control recording before appearance of this loop not available from this cell); (*B*) equivalent recording as *A* but ≈1 min later, characteristic loop more expressed; (*C*) equivalent recording as *B* but ≈1 min later; one out of three equivalent recordings taken within 1 min (Gradmann and Boyd, 1999). (*D–G*) Fits to current differences at $V \leq -80$ mV; (*D*) current differences *B-A*, showing temporal outward current in the descending (*V* ramp from + to −) branch; dots: experimental data, line fitted with *V*-gated G_P with three-state (*1-2-3*) gating model ($1 = i_1$, $2 = a$, $3 = i_2$) and; parameters listed in Table 5, start configuration for Fit: 1111 in Table 5.*D′* better resolution of *D* showing intersection at about −170 mV with flat, ascending (*V* ramp from − to +) branch, and decreasing activity at the negative turning point, i.e., amount of current before the turning point larger than after; (*E*) apparent tilt of linear ascending branches between *C* and *B* indicates (loss of) leak conductance ($G_L = -1$ μS); (*F*) current differences *C-B*, showing superposition of G_L and *V*-triggered G_{Cl} transient (V_X*:* trigger point); dots: experimental data, line fitted with G_L plus $G_{Cl}(t) = G_{Cl,max}X(t)$ according to Eq. 1; parameters in Table 5. (*G*) current differences between recording *C* and *A*, displaying isolated and total *I-V-t* relationship of Type-III excitation; dots recorded, line fitted with *V*-triggered G_{Cl} transient (V_X*:* trigger point) and *V*-gated G_P*;* parameters listed in Table 4, start configuration for fit: 1111 in Table 5.

eters show little variation (e.g., k^0_{23}) and some more (e.g., k^0_{32}). This issue has been investigated again systematically for Type-III excitations. The data in Table 4 show that various parameter configurations, as obtained with different sets of start parameters, result in fits of the same high quality (SD of σ only about 0.1%) which cannot be distinguished by visual inspection. Table 4 shows also that this variability is not the same for each parameter; e.g., k^0_{23} reliably converged to 0.24 sec^{-1}, whereas k^0_{23} tended to diverge arbitrarily. This issue is confirmed by Table 6 which shows how much the fit quality decreases when the individual parameters deviate by 1% from the fitted optimum. Again, k^0_{32} (and d_{32} consistently) have almost no effect on the fit quality. On the other hand,

Table 4. Stability of fitted *k* values with respect to configuration of start values in fits of gating scheme *1-2-3* for pump activity in Type-III excitation: *1* = i_1, *2* = *a*, *3* = i_2; for data in Fig. 2*C-A*

Parameter Reference	Gated pump				G_{Cl} transient			
	k^0_{12} 0.3	k^0_{21} 10000	k^0_{23} 0.3	k^0_{32} 0.3	k_r 3	k_b 1	σ_{start}	σ_{stop}
Start confg. Fitted								
1111	0.35	9840	0.24	0.4	2.97	0.88	18	15.44
2111	0.45	13082	0.23	0.4	2.98	0.88	25	15.42
1211	0.45	12909	0.24	0.5	2.98	0.88	27	15.41
2211	0.50	14783	0.23	0.4	2.98	0.86	18	15.43
1121	0.34	9362	0.24	0.8	2.97	0.87	27	15.43
2121	0.35	9950	0.24	0.8	2.97	0.87	31	15.42
1221	0.38	10900	0.24	0.8	2.98	0.87	34	15.40
2221	0.39	11119	0.24	0.8	2.98	0.87	27	15.40
1112	0.35	9754	0.24	0.8	2.97	0.87	18	15.42
2112	0.46	13213	0.24	0.8	2.98	0.87	25	15.40
1212	0.44	12623	0.24	0.9	2.97	0.86	27	15.39
2212	0.51	15137	0.23	0.8	2.97	0.84	18	15.42
1122	0.34	9444	0.24	1.5	2.96	0.86	27	15.40
2122	0.37	10506	0.24	1.5	2.96	0.86	31	15.38
1222	0.39	11036	0.24	1.4	2.98	0.87	34	15.38
2222	0.40	11499	0.24	1.5	2.97	0.85	27	15.37
111121	0.36	10000	0.24	0.3	2.98	0.89	76	15.44
111112	0.27	10367	0.24	0.2	2.98	0.89	38	15.44
Means (1111 to 2222)	0.40	11566	0.238	0.9	2.97	0.87	27	15.41
SD/%	13	16	2	45	0.2	1.2	21	0.1

k in sec^{-1}; σ in nA; code for configuration of start parameters: factors of standard configuration, e.g., 2112 means $k^0_{12} = 0.6$, $k^0_{21} = 10{,}000$, $k^0_{23} = 0.3$, $k^0_{12} = 0.6$ sec^{-1}; in 111121 and 11112, start parameters of k_r and k_b have also been doubled, respectively; fixed parameters: $E_P = -165$ mV, $G_{P,max} = 10$ μS, $d_{12} = -1$, $d_{21} = 1$, $d_{23} = -0.5$, $d_{32} = 0.5$, $G_{Cl,max} = 10$ nS, $V_X = -180$ mV, $k_r = 10$ sec^{-1}, $k_b = 10$ sec^{-1}, $G_L = 1$ μS; start increment: ±1%, stop increment: ±0.1%.

Table 5. Model parameters for series of Type-III excitations from one cell, determined from fits of differences in Fig. 5

Start	Gated pump				G_{Cl} transient			
	k^0_{12} 0.3	k^0_{21} 10 000	k^0_{23} 0.3	k^0_{32} 0.3	k_r 3.0	k_b 1.0	σ_{start}	σ_{stop}
Fig. 5 fit								
B-A	0.30	9 280	0.23	0.21	—	—	14.7	12.44
C-B	—	—	—	—	2.87	1.01	11.9	10.76
C-A	0.35	9 840	0.24	0.39	2.97	0.88	17.7	15.44
(C-A)′	0.303	15 880	0.204	1.262	3.622	0.843	15.40	7.44

Fits to current differences at $V \leq -80$ mV; *k* in sec^{-1}; σ in nA; gating scheme *1-2-3* for *pump: 1* = i_1, *2* = *a*, 3 = i_2; fixed parameters: $E_P = -165$ mV, $G_{P,max} = 10$ μS, $d_{12} = -1$, $d_{21} = 1$, $d_{23} = -0.5$, $d_{32} = 0.5$, $V_X = -180$ mV, $G_{Cl,max} = 10$ nS, $G_L = -1$ μS; start increment: ±1%, stop increment: ±0.1%; (*C-A*)′: all parameters free: fixed parameters and mean fitted parameters from Table 4 used as start parameters, start increment 0.1%; stop increment 0.01%, additional fitted parameters: $E_P = -171.3$ mV, $G_{P,max} = 11.36$ μS, $d_{12} = -1.086$, $d_{21} = -1.054$, $d_{23} = -0.534$, $d_{32} = 0.345$, $G_{Cl,max} = 8.12$ nS, $V_X = -187.8$ mV, $G_L = -689$ nS.

Table 6. Differential sensitivity of S of fit quality on changes of individual parameters, P, of model for Type-III excitations; reference parameters fitted with start configuration 1111 (s. Table 4)

Gated pump											G_{Cl} transient				Leak
P	E_P	G_P	k^0_{12}	d_{12}	k^0_{21}	d_{21}	k^0_{23}	d_{23}	k^0_{32}	d_{32}	V_X	G_{Cl}	k_r	k_b	G_L
S	30	0.7	0.2	5	2	3	0.2	2	—	—	60	7	3	0.2	4

S: arithmetic mean of increase in σ (in ‰) upon a ±1% change of particular parameter value; −: <0.1.

variations of the parameters V_X, E_P, G_{Cl} and G_L for instance, have large effects on the fit quality. For this reason, these parameters could be approximated beforehand and be used later as fixed parameters.

Comparative Aspects

According to the current dogma, the role of Na^+ channels in the animal action potential is replaced by Cl^- channels in the action potential of plant membranes because many excitable plant cells lack Na^+ in their external medium and voltage-gated Na^+ channels are virtually absent in plants (Sanders & Slayman 1989). In evolutionary terms, however, the other way around appears to be more likely, because electrical excitation in the common ancestors of plants and animals was probably more of the Cl^- type (and involved in osmoregulation) than of the osmotically neutral type of action potentials in animals (Gradmann & Mummert, 1979). However, this appealing analogy of Cl^- channels and Na^+ channels does not stand a rigorous examination. The current evidence from green algae (e.g., Thiel, Homann & Gradmann, 1993, Biskup et al., 1999) and diatoms (this study) indicates that the *V*-induced G_{Cl} transients in plant excitation are not primarily due to *V*-gating of Cl^- channels but are mediated by a *V*-triggered messenger (Ca^{2+}). Interestingly G_{Cl} has been demonstrated to contribute to the excitation of olfactory sensory neurons of vertebrates (Reuter et al., 1998), and this Cl^- conductance has recently been reported to be gated not by *V* directly but by the *V*-triggered messenger Ca^{2+} (Sato & Suzuki 2000). This corresponds closely to the role of G_{Cl} in the plant action potentials of the fresh-water cells of *Chara* (Biskup et al., 1999) and of the marine cells of *Coscinodiscus* (this study), assuming that Ca^{2+} is here the messenger as well.

Conclusions

(i) Single saw-tooth clamp is a powerful method to record nonlinear *I-V-t* relationships in a short time.

(ii) The data from these recordings are, in principle, suited to determine the parameters of Markovian models for voltage-gated conductances.

(iii) At least three distinct types of electrical excitation occur in the marine diatom *C. wailesii.*

(iv) All three types employ a transient G_{Cl}, mediated by a *V*-triggered messenger.

(v) *V*-gated pump activity plays the key role in a novel, hyperpolarization-type of excitation.

(vi) It is too early to speculate about specific physiological functions to the distinct types of excitation. Nevertheless, we note that Type-I and Type-II excitations comprise a net loss of salt and water (osmotically), and consequently result in an overall increase of the density of the cell (towards the density of dry proteins and silica). These mechanisms may play a role in regulation of the buoyancy in marine diatoms.

(vii) The variety of distinct types of electrical excitations presented here widens the scope of excitability of biomembranes from familiar action potentials (best known in animals) to a more general issue in membrane biology:

(viii) We suggest that the original function of electrical excitability of biological membranes is related to osmoregulation which has persisted through evolution in plants, whereas the familiar and osmotically neutral action potentials in animals have evolved later towards the novel function of rapid transmission of information over long distances.

We thank Drs. Ulrike Homann and Gerhard Thiel for critical reading of the manuscript. Research of C.M.B. has been supported by grants from the Natural Sciences—Engineering Research Council of Canada.

References

Biskup, B., Gradmann, D., Thiel, G. 1999. Calcium release from $InsP_3$-sensitive internal stores initiates action potential in *Chara. FEBS Lett.* **453:**72–76

Boyd, C.M., Gradmann, D. 1999. Electrophysiology of the marine diatom *Coscinodiscus wailesii* I: Endogenous changes of membrane voltage and resistance. *J. Exp. Bot.* **50:**445–451

Grabov, A., Blatt, M.R. 1998. Membrane voltage initiates Ca^{2+} waves and potentiates Ca^{2+} increases with abscisic acid in stomatal guard cells. *Proc. Natl. Acad. Sci. USA* **95:**4778–4783

Gradmann, D., Blatt, M.R., Thiel, G. 1993. Electrocoupling of ion transporters in plants. *J. Membrane Biol.* **136:**327–332

Gradmann, D., Boyd, C.M. 1995. Membrane voltage of marine phytoplankton, measured in the diatom *Coscinodiscus radiatus. Marine Biology* **123:**645–650

Gradmann, D., Boyd, C.M. 1999. Electrophysiology of the marine diatom *Coscinodiscus wailesii* IV: Types of non-linear current-voltage-time relationships recorded with single saw-tooth voltage-clamp. *Eur. Biophys. J.* **28:**591–599

Gradmann, D., Hoffstadt, J. 1998. Electrocoupling of ion transporters in plants: Interaction with internal ion concentrations. *J. Membrane Biol.* **166:**51–59

Gradmann, D., Mummert, H. 1980. Plant action potentials. *In:* Plant Membrane Transport: Current Conceptual Issues. R.M. Spanswick, W.J. Lucas, and J. Dainty, editor., pp. 333–344. Elsevier Biomedical Press, Amsterdam

Mummert, H., Gradmann, D. 1991. Action potentials in *Acetabularia:* measurement and simulation of voltage-gated fluxes. *J. Membrane Biol.* **124:**264–272

Ohkawa, T., Kishimoto, U. 1975. Anode break excitation in *Chara* membrane. *Plant & Cell Physiol.* **16:**83–91

Reuter, D., Zierold, K., Schroeder, W.-H., Frings, S. 1998. A depolarizing chloride current contributes to chemoelectrical transduction in olfactory sensory neurons in situ. *J. Neurosc.* **18:**6623–6630

Sanders, D., Slayman, C.L. 1989. Transport at the plasma membrane of plant cells: a review. Plant Membrane Transport: The Current Position. *In:* J. Dainty et al., editor. pp. 1–11. Elsevier, Amsterdam

Sato, K., Suzuki, N. 2000. The contribution of a Ca^{2+} activated Cl^- conductance to amino-acid induced inward current responses of ciliated olfactory neurons of the rainbow trout. *J. Experimental Biology.* **203:**253–262

Thiel, G., Homann, U., Gradmann, D. 1993. Microscopic basis of electrical excitation in *Chara:* transient activity of Cl^- channels in the plasma membrane. *J. Membrane Biol.* **134:**53–66

Werner, D. 1977. The Biology of Diatoms. *Botanical Monographs* **13:**1–17